 DOI: 10.30420/566262350

Comparison of Two Bidirectional 11KW 400V CLLC and CLLLC Resonant Converters for EV Applications

Hasan Mousavi Somarin[1], Norbert Messi[2], Farshid Sarrafin Ardebili[3], Luiz Braz[4]

[1,2,3,4] Valeo Systèmes De Contrôle Moteur, France

Corresponding author: Hasan Mousavi Somarin, hasan.mousavi-somarin@valeo.com
Speaker: Hasan Mousavi Somarin, hasan.mousavi-somarin@valeo.com

Abstract

Resonant converters are becoming increasingly popular due to their lower power loss, higher efficiency, improved electromagnetic interference (EMI) characteristics, and better bi-directional performance. To transfer power bi-directionally, it is necessary to have two resonant tanks on both the primary and secondary sides of the transformer. Two types of resonant topologies, namely, CLLC and CLLLC, are widely used in the EV sector. This paper aims to compare these two converters in terms of power loss, component count, operation, EMC behavior, volume, and efficiency. This way, the design process for two 11 kW 400 V CLLC and CLLLC converters is presented, and a comprehensive comparison is provided.

1 Introduction

Resonant converters have mostly emerged as prominent choices within the Electric Vehicle (EV) sector, particularly in the realm of onboard chargers. Renowned for their superior efficiency compared to other converter types, these DC/DC converters play a pivotal role in enhancing the charging infrastructure of EVs. While the design of resonant converters has evolved considerably over recent years, reaching a level of maturity, the pursuit of optimization remains a focal point of ongoing research. Despite significant advancements, there exists a continued interest in refining and fine-tuning these converters to maximize their performance in real-world EV applications.

In [1], a planar integrated transformer design for energy storage systems is introduced. However, the analysis lacks discussion on parasitic parameters and electromagnetic interference (EMI) behavior of the converter. Notably, factors such as complex manufacturing, limited power handling, higher cost, and sensitivity associated with planar transformers often favor the use of conventional transformers in many applications.

In [2], a Gallium Nitride (GaN) based CLLC resonant converter is developed, boasting an impressive efficiency of 97.02%. Additionally, [3] proposes a control strategy aimed at stabilizing the CLLLC resonant converter. However, there remains a lack of clarity regarding which topology, in terms of resonant capacitors and inductors, is optimal for specific applications.

A comprehensive survey on resonant tanks is conducted in [4], while [5] presents a comparison between two 3.5KW CLLC and CLLLC resonant converters, albeit with separately designed inductors and transformers in both cases.

In our current study, we focus on two 11KW 400V bidirectional CLLC and CLLLC converters, examining, designing, and comparing their performance. For the CLLC converter, we design the separated inductor and a transformer, whereas in the CLLLC converter, the leakage inductance of the transformer is utilized as the series resonant inductance [6-8]. In both cases, the magnetizing inductances serve as the parallel resonant inductance [9].

In typical electromagnetic designs, integrated transformer-inductors often feature separate winding types to achieve the required leakage inductance [10-12]. Consequently, high-frequency AC copper loss becomes unavoidable in such designs. Notably, the distinctive feature of our designed CLLLC transformer-inductor lies in its interleaved winding type, a rarity among integrated transformer-inductors. This design choice significantly reduces AC copper loss, thereby contributing to enhanced efficiency.

The subsequent sections of this paper delve into the modeling of the CLLC and CLLLC converters. Gain curves for both topologies are provided and compared, offering insight into their respective performances. Additionally, the transient behavior of both converters is analyzed and compared.

Furthermore, the paper details the design process of electromagnetic components, which are pivotal in resonant converters. A comparative study is conducted between two types of electromagnetic parts: separately designed transformers and inductors versus integrated transformer and inductor configurations.

ISBN 978-3-8007-6262-0

Finally, the test results are presented, accompanied by an efficiency comparison between the two converter topologies.

2 Modelling

2.1 Schematic diagram

Figure 1 illustrates the schematic diagram of CLLLC and CLLC resonant converters. The gain function for these converters is obtained using the First Harmonic Approximation (FHA) method.

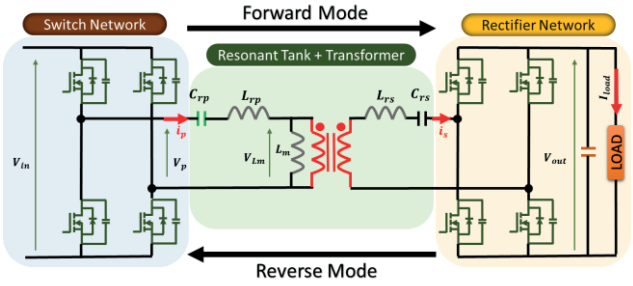

CLLLC resonant converter

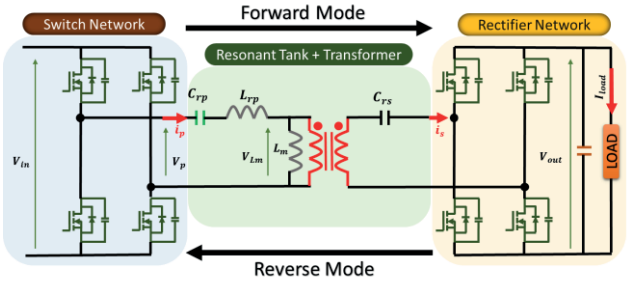

CLLC resonant converter

Figure 1. Schematic diagram of two 11KW 400V bidirectional resonant converter.

In the FHA approach, the primary side switch network, typically found in an inverter generating a quasi-sine voltage waveform, is replaced by its equivalent voltage source. For the primary side, the fundamental or first harmonic of the voltage at the resonant frequency equals (4/π) times the maximum DC voltage, denoted as Vx.

On the secondary side, both the rectifier network and the DC load are substituted with their equivalent AC load. The equivalent AC load value is calculated as $R_{ac} = (8/\pi^2)n^2R_{DC}$ where n represents the transformation ratio.

Figure 2 illustrates the FHA model of the CLLLC and CLLC resonant converters. Parameters labeled with "PRIM" signify elements transferred to the primary side of the transformer.

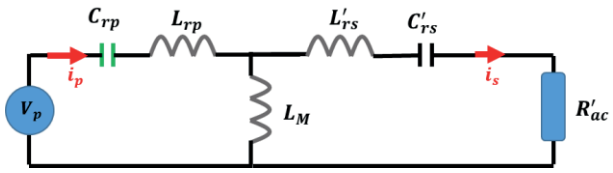

FHA model of CLLLC converter

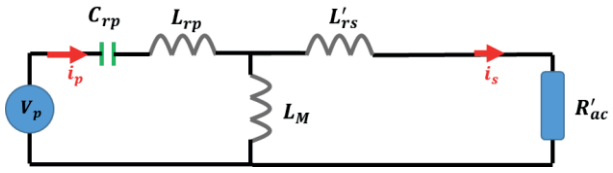

FHA model of CLLC converter

Figure 2. Simplified FHA model of two 11KW 400V bidirectional resonant converter

2.2 Mathematical model

The mathematical model of the converters can be found in [2] and [13]. Here, we present only the final gain functions.

The gain function of the CLLLC converter for the forward and reverse modes are as follows:

$$G_f(F_n) = \frac{1}{\sqrt{\left(1+\frac{1}{\lambda}-\frac{1}{\lambda F_n^2}\right)^2+Q^2\left(\frac{1}{\lambda g_c F_n^3}+F_n+\frac{g_L F_n}{\lambda}-\frac{1}{F_n}-\frac{g_L}{\lambda F_n}-\frac{1}{\lambda g_c F_n}-\frac{1}{g_c F_n}\right)^2}} \quad (1)$$

$$G_r(F_n) = \frac{1}{\sqrt{\left(1+\frac{1}{\lambda'}-\frac{1}{\lambda' F'^2_n}\right)^2+Q'^2\left(\frac{1}{\lambda' g_c' F'^3_n}+F'^3_n+\frac{g_L' F'_n}{\lambda'}+g_L' F'_n-\frac{1}{F'_n}-\frac{g_L'}{\lambda'}-\frac{1}{\lambda' g_c' F'_n}-\frac{1}{g_c' F'_n}\right)^2}} \quad (2)$$

Where $F_{res-f} = \frac{1}{2\pi\sqrt{L_{rp}\ C_{rp}}}$ is the Resonant frequency in the forward mode, $F_{res-r} = \frac{1}{2\pi\sqrt{L_{rs}\ C_{rs}}}$ is the Resonant frequency in the reverse mode, $F_n = \frac{F_{switching}}{F_{res-f}}$ is the Normalized frequency in the forward mode, $F'_n = \frac{F_{switching}}{F_{res-r}}$ is the Normalized frequency in the reverse mode, $Q = \frac{\sqrt{\frac{L_{rp}}{C_{rp}}}}{R_{ac}}$ is the quality factor in the forward mode, $Q' = \frac{\sqrt{\frac{L_{rs}}{C_{rs}}}}{R_{ac}}$ is

ISBN 978-3-8007-6262-0

the quality factor in the reverse mode, $g_L = \frac{C'_{rs}}{C_{rp}}$ is the capacitance ratio in the forward mode, $g_c{}' = \frac{C'_{rp}}{C_{rs}}$ is the capacitance ratio in the reverse mode, $\lambda = \frac{L_M}{L_{rp}}$ is the inductance ratio in the forward mode, and $\lambda = \frac{L_M}{L_{rs}}$ is the inductance ratio in the reverse mode

The gain function of the CLLC converter for the forward and reverse modes are

$$\|G_F\| = \| \frac{nV_o}{V_{F_{tank}}} \| = \| \ 1 + \frac{f^2-1}{L_n \ f^2} + j\left\{ \frac{Q_1\left[C_n L_n f^4 - (C_n L_n + L_n + 1) f^2 + 1\right]}{C_n L_n f^3} \right\} \|^{-1} \quad (3)$$

$$\|G_R\| = \| \frac{V_o}{nV_{R_{tank}}} \| = \|1 - \frac{1}{C_n L_n \ f^2} + j\left\{ \frac{Q_2\left[C_n L_n f^4 - (C_n L_n + L_n + 1) f^2 + 1\right]}{\sqrt{C_n} L_n f^3} \right\} \|^{-1} \quad (4)$$

Where

$Q_1 = \frac{\sqrt{L_{rp}/C_{rp}}}{R'_{F_{ac}}}$ is the quality factor in the forward mode, $Q_2 = \frac{\sqrt{L_{rs}/C_{rs}}}{R'_{R_{ac}}}$ is the quality factor in the reverse mode, $C_n = \frac{C'_{rs}}{C_{rp}}$ is the capacitance ratio in the forward mode, $L_n = \frac{L_m}{L_{rp}}$ is the inductance ratio in the forward mode, $f_n = \frac{1}{2\pi\sqrt{L_{rp}C_{rp}}}$ is the basic frequency, $f = \frac{f_s}{f_n}$ is the normalized operating frequency, $f_{m1} = \frac{1}{2\pi\sqrt{(L_{rp}+L_m)C_{rp}}}$ is the Series inverter-side resonant frequency in the forward mode, and $f_{m2} = \frac{1}{2\pi\sqrt{L_m C'_{rs}}}$ is the Series inverter-side resonant frequency in the reverse mode

Unlike the CLLLC topology, the CLLC topology is not symmetrical; therefore, there will be two Quality Factors and two resonant frequencies in the forward and reverse modes of operation. Defining the $a = C_n L_n$ and $b = -(C_n L_n + L_n + 1)$, the normalized resonant frequencies for the forward mode f_{resF} and reverse mode f_{resR} will be

$$f_{resF} = \sqrt{\frac{-b-\sqrt{b^2-4a}}{2a}} \quad (5)$$

$$f_{resR} = \sqrt{\frac{-b+\sqrt{b^2-4a}}{2a}} \quad (6)$$

2.3 Designing the resonant tank

To design the resonant tank, gain curves of the resonant converters are plotted for various values of the Quality factor (Q) and inductance ratio (λ or Ln). Subsequently, from these curves, the gain curve that satisfies the minimum and maximum gain values is selected.

Once the Q and Ln values are determined from the plots, and with the resonant frequency (120 kHz) from the input data, three known parameters and three unknown parameters are identified. Consequently, a system of three Equations is formulated. By solving this system, the values of the resonant capacitances, series resonant inductances, and the parallel (magnetizing) inductance can be calculated.

2.4 Validation of the resonant tank size

The effectiveness of the selected parameters is validated through the AC simulation in the first step.

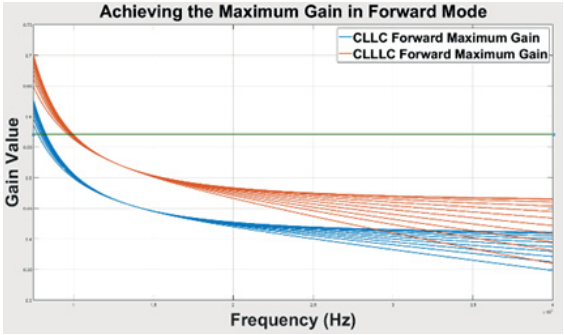

ISBN 978-3-8007-6262-0

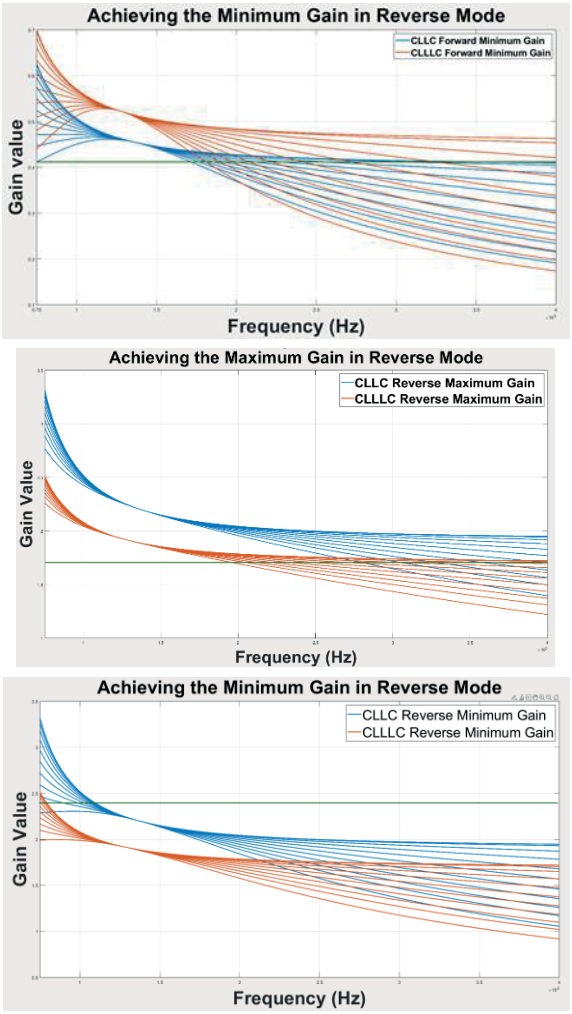

Figure 3. Achieving the minimum and maximum gain in forward and reverse modes of operation in the worst case condition. Red curves: CLLLC converter gain curves from 0.5KW to 10.5KW; blue curves: CLLC converter gain curves from 0.5KW to 10.5KW

Figure 3 depicts the gain curves of the CLLLC and CLLC converters in both forward and reverse modes of operation, spanning load values from 0.5 kW to 10.5 kW. Each plot includes a horizontal line indicating the critical value of the gain.
Observations reveal that in the forward mode, the CLLLC converter exhibits a higher gain compared to the CLLC converter. Conversely, in the reverse mode, this relationship is reversed. Notably, the resonant frequency in the CLLC converter is slightly shifted to the left.
Under forward operation, the CLLC converter can achieve slightly higher power output compared to the CLLLC converter for the same inductance value. However, when the output voltage decreases, the CLLLC converter demonstrates superior response. Despite both converters being capable of reaching the minimum gain in the forward mode, the CLLC variant operates at lower frequencies, deviating significantly from the resonant frequency and resulting in higher harmonics. In the reverse mode, the CLLLC converter outperforms the CLLC converter in achieving both minimum and maximum voltages. Notably, the CLLLC converter exhibits less deviation when achieving maximum gain, leading to fewer harmonics, improved Zero Voltage Switching (ZVS), and increased efficiency.

2.5 Transient simulation

To assess the voltage and current stress on c omponents of the converters, transient simulati ons were conducted. The results of these sim ulations, reflecting the four modes of operatio under worst conditions, are presented in Table s 1 through 4, where V_Crp and V_Crs are the applied voltage to the primary and secondary resonant capacitor networks respectively, I_rp and I_rs are the current passing through the primary and secondary capacitor networks respectively, V_tr_p and V_tr_s are the applied voltage to the primary and secondary side windings, Fsw is the switching frequency and I_mos_P and I_mos_S are the current passing through primary and secondary MOSFETs.

2.5.1 Achieving the minimum gain in forward mode

650V ->270V	5KW		8KW		10.5KW	
	CLLLC	CLLC	CLLLC	CLLC	CLLLC	CLLC
V_Crp(V)	85	95	160	164	224	220
V_Crs(V)	36	44	71	80	101	111
I_rp(A)	11	10	18	16	23	21
I_rs(A)	20	19	32	31	42	41
V_tr_p(V)	705	707	758	748	805	782
V_tr_s(V)	269	272	274	279	283	290
Fsw (KHz)	214	174	179	157	166	150
I_mos_P(A)	8	7	12	11	16	14
I_mos_S (A)	14	13	22	22	29	29

Table 1. Voltage and current stress of the components in CLLLC and CLLC converters in different operating point while achieving the minimum voltage in forward mode

ISBN 978-3-8007-6262-0

The comparison reveals that, in this operational point, the CLLLC converter experiences higher voltage and current stress on both the primary and secondary resonant capacitors compared to the CLLC converter. Additionally, the applied voltage to the primary side of the transformer in the CLLLC converter is slightly lower than that of the CLLC converter, leading to reduced core losses in the transformer.
Furthermore, the CLLC converter operates at a lower switching frequency compared to the CLLLC converter under the same operating conditions, resulting in decreased switching losses. Lastly, the primary and secondary MOSFET switches in the CLLLC converter exhibit lower current stress than those in the CLLC converter, leading to reduced conduction losses.

2.5.2 Achieving the Maximum gain in forward mode

820 --> 470 V	5KW		8KW		10.5KW	
	CLLLC	CLLC	CLLLC	CLLC	CLLLC	CLLC
V_Crp(V)	163	269	215	275	292	309
V_Crs(V)	52	65	84	107	112	142
I_rp(A)	10	14	13	14	16	16
I_rs(A)	13	13	21	23	28	30
V_tr_p(V)	818	1048	945	1013	947	996
V_tr_s(V)	445	436	446	437	449	439
Fsw (KHz)	99	82	98	81	98	80
I_mos_P(A)	7	10	9	10	11	16
I_mos_S (A)	9	9	15	16	19	30

Table 2. Voltage and current stress of the components in CLLLC and CLLC converters in different operating point while achieving the maximum voltage in forward mode

In this specific operating point, it is observed that the CLLLC converter exhibits lower voltage and current stress on both the primary and secondary resonant capacitors compared to the CLLC converter. This reduction in stress results in lower power losses.
Moreover, the applied voltage to the primary side of the transformer in the CLLLC converter is lower than that of the CLLC converter, leading to decreased core losses.
While the CLLLC converter operates at a higher switching frequency compared to the CLLC converter, contributing to increased switching losses, it switches near the resonant frequency. This facilitates Zero Voltage Switching (ZVS) and results in fewer harmonics.
Lastly, the current stress experienced by the primary and secondary MOSFET switches in the CLLLC converter is lower than that of the CLLC converter, leading to reduced conduction losses.

2.5.3 Achieving the Maximum gain in reverse mode

470 --> 820 V	5KW		8KW		10.5KW	
	CLLLC	CLLC	CLLLC	CLLC	CLLLC	CLLC
V_Crp(V)	60	38	100	75	141	108
V_Crs(V)	45	29	63	53	85	73
I_rp(A)	6	6	10	10	13	14
I_rs(A)	19	20	26	30	33	37
V_tr_p(V)	801	782	803	793	787	796
V_tr_s(V)	505	493	514	511	825	525
Fsw (KHz)	171	270	164	218	155	203
I_mos_P(A)	4	4	7	7	9	10
I_mos_S (A)	13	14	18	21	23	26

Table 3. Voltage and current stress of the compone nts in CLLLC and CLLC converters in different oper ating point while achieving the maximum voltage in reverse mode

At this specific operating point, certain differences in voltage and current stress between the CLLLC and CLLC converters are observed. The voltage stress in the CLLLC converter is higher compared to the CLLC converter, while the current stress remains slightly higher in the CLLC converter, resulting in comparatively higher power losses.
The applied voltage to the primary side of the transformer is approximately the same in both converters, making it difficult to definitively determine whether core losses are decreased or increased.
Although the switching frequency of the CLLLC converter is lower than that of the CLLC converter, resulting in less switching loss, it operates close to the resonant frequency, thereby reducing harmonics.
Lastly, the overall current in the primary and secondary MOSFET switches is slightly decreased in

ISBN 978-3-8007-6262-0

the CLLLC converter, leading to comparatively higher conduction losses on these switches.

2.5.4 Achieving the Minimum gain in reverse mode

270 --> 650 V	5KW		8KW		10.5KW	
	CLLLC	CLLC	CLLLC	CLLC	CLLLC	CLLC
V_Crp(V)	201	133	328	215	434	283
V_Crs(V)	114	89	168	128	225	165
I_rp(A)	10	9	17	15	23	19
I_rs(A)	23	24	35	35	46	46
V_tr_p(V)	581	619	565	619	583	633
V_tr_s(V)	329	319	320	321	326	328
Fsw (KHz)	78	110	77	109	77	109
I_mos_P(A)	7	6	12	10	23	14
I_mos_S (A)	16	17	24	35	46	32

Table 4. Voltage and current stress of the components in CLLLC and CLLC converters in different operating point while achieving the minimum voltage in reverse mode

In this operating point, it is observed that the voltage and current stress on the primary and secondary resonant capacitors in the CLLLC converter are higher compared to the CLLC converter, consequently leading to increased power loss. Additionally, the applied voltage to the primary winding of the transformer is lower in the CLLLC converter, resulting in reduced core loss. Although the switching frequency in the CLLLC converter is lower than that of the CLLC converter, the latter switches near resonance, exhibiting fewer harmonics in this particular operating point. Finally, while the current flowing through the primary side MOSFET switches in the CLLLC converter is generally lower in most operating points, it is comparatively higher in the secondary MOSFET switches.

3 Electromagnetics design

In this section, we will delve into the design of three key electromagnetic components. Specifically, we will discuss the design and construction of an inductor and a transformer with a predetermined value of magnetizing inductance for the CLLC converter, where the magnetizing inductance serves as the parallel inductor. Additionally, for the CLLLC converter, we will detail the design of an integrated transformer-inductor. In this design, the leakage inductance is utilized as the series resonant inductance, while the magnetizing inductance is tailored to function as the parallel inductor. It's important to note that due to confidentiality reasons, the detailed specifications of these components cannot be disclosed.

3.1 Core sizing

The **Area Product (A_p)** approach is a commonly utilized method for determining the size of transformer and inductor cores. Equation (7) and Equation (8) are employed in this context to calculate the size of the transformer and inductor cores, respectively.

$$A_p = A_w A_e = \frac{2 \times P_o}{K_f \ K_u \ f \ B_{max} \ J} \quad (7)$$

$$A_p = A_w A_e = \frac{L \ I_{max}^2}{K_u \ B_{max} \ J} \quad (8)$$

Where A_w is the window area in which the windings will be winded, A_e is the cross-sectional area of the core, P_o is the output power (KW), K_f is the waveform coefficient: 4 for square waves and 4.44 for sinusoidal ones, K_u is the utilization or filling factor, f is the minimum frequency, B_{nax} is the maximum flux density, J is the maximum current density, L is the inductance, and I_{max} is the inductor's peak current.
Once the core size is calculated, referring to the core manufacturer a suitable size core can be selected. To optimize the power loss and volume the size and geometry of the core can also be customized. For the current design, the shape and size of the core for all three components are customized.

3.2 Number of turns

Equation (9) and (10) will be used to determine the number of turns for transformer and inductor respectively.

$$N_1 = \frac{V_p \ D}{2 B_{max} \ f \ A_e} \quad (9)$$

$$N_{ind} = \sqrt{\frac{L}{A_L}} \quad (10)$$

Where
N_1 is the number of the turns of transformers' primary winding. The secondary will be caluculated using the transformation ratio
V_p is the primary peak voltage, which is equal to

$$\frac{4}{\pi} V_{dc-max} = \frac{4}{\pi} \times 820 = 1044.1V$$

ISBN 978-3-8007-6262-0

D is the duty ratio which is equal to 0.5 in this design
N_{ind} is the turn number of the inductor
L is the inductance
A_L is the specific inductance value of the core provided by the supplier

3.3 Conductor sizing

The bare conductor diameter d_{bare} for the primary and secondary of the transformer, as well as for the inductor, is computed individually using the Equation (11).

$$d_{bare} = \sqrt{\frac{4\ I_{RMS}}{\pi\ J}} \qquad (11)$$

Where
I_{RMS} is the worst case RMS current

3.4 Skin and proximity effects

Given that the intended converter operates at high frequencies, it is essential to consider skin and proximity effects. The skin depth is determined using Equation (12).

$$\delta = \sqrt{\frac{\rho_{copper\ @\ 100℃}}{\pi\ \ \mu_0\ \mu_r\ f_{sw}}} \qquad (12)$$

Where
$\rho_{copper\ @\ 100℃}$ is the copper resistivity at $100℃$
μ_0 is the vacuum or free space permeability
μ_r is the copper permeability
f_{sw} is the switching frequency
In high-frequency applications, it is crucial for the skin depth to be larger than the conductor diameter d_{bare} . If this condition is not met, it becomes imperative to utilize Litz wire to mitigate the skin effect effectively. Moreover, implementing interleaved winding techniques helps reduce the proximity effect, leading to a notable reduction in AC copper loss.

3.5 Gap length

The minimum length of the air gap g_{min} is determined using Equation (13).

$$g_{min} = N^2 \frac{\mu_0\ \ A_e}{L} \qquad (13)$$

In Equation (13), N represents the number of turns for the inductor or, in the case of transformer design; it denotes the number of turns in the transformer's primary winding. For the inductor, L corresponds to the desired inductance value. For the transformer, L represents the magnetizing inductance value, while for the integrated transformer-inductor, L is the sum of the magnetizing inductance and sum of the primary and secondary leakage inductances.

4 Comparison

The designed transformer, inductor, and integrated transformer-inductor are subjected to simulation using Ansys Maxwell, a 3D FEM electromagnetic simulation tool. Various types of simulations, namely Magneto-static, Eddy Current, Transient and Electro-static, are conducted to validate the parameters.
Following each simulation, feedback from the results is utilized to refine and redesign the components as necessary. This iterative process ensures that the final designs meet the desired performance specifications. In the subsequent analysis, we will compare two topologies: one employing separate inductor and transformer components (CLLC), and the other utilizing an integrated transformer-inductor configuration (CLLLC).

4.1.1 Resistance

	CLLC			CLLLC	
	Transformer		Inductor	Integrated Transformer-Inductor	
	Primary	Secondary		Primary	Secondary
Rdc (mΩ)	34	38	15	35	39
Rac(mΩ) @75KHz	48	44	17	41	45
Rac(mΩ) @100KHz	57	52	18	45	50
Rac(mΩ) @200KHz	125	109	28	74	84
Rac(mΩ) @250KHz	176	151	36	96	109

Table 5. AC resistance of the separated and integrated transformer-inductor

The comparison reveals that the AC resistance of the integrated transformer-inductor is lower than that of the separated transformer and inductor configuration. Consequently, it is anticipated that the integrated transformer-inductor will experience lower copper losses compared to the separated components.

4.1.2 Core loss at nominal power

	CLLC	CLLLC

ISBN 978-3-8007-6262-0

	Transformer	Inductor	Integrated Transformer-Inductor
Core loss (W) @75KHz	2.3	0.9	2.3
Core loss (W) @100KHz	6.4	2.5	6.4
Core loss (W) @200KHz	72	27	72
Core loss (W) @250KHz	158	60	158

Table 6. Core loss of the separated and integrated transformer-inductor

The separated transformer and inductor configuration exhibits higher core volume, leading to increased core losses. Conversely, integrating the inductor into the transformer has effectively reduced the core losses.

4.1.3 Parasitic parameters

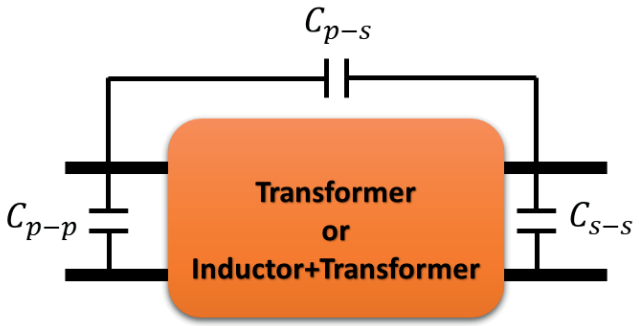

Figure 4. Parasitic elements in electromagnetics

Figure 4 illustrates the parasitic elements of the CLLC/CLLLC electromagnetic components, where C_{p-p} and C_{s-s} represent the primary and secondary winding parasitic capacitances, respectively, and C_{p-s} denotes the intertwining capacitance between the primary and secondary windings. Corresponding parasitic parameter values are presented in Table 7. Analysis of these parameters suggests that the EMI behavior of the CLLLC configuration is anticipated to outperform that of the CLLC.

	C_{p-p} (pF)	C_{s-s} (pF)	C_{p-s} (pF)
CLLC	2.03	1.27	257.79
CLLLC	1.5	2.65	64.6

Table 7. Parasitic capacitance values of CLLC and CLLLC electromagnetic components

4.1.4 Volume

	CLLC	CLLLC

	Transformer	Inductor	Integrated Transformer-Inductor
Total Core volume (mm^3)	67706	36989	68371
Total Copper volume (mm^3)	20056	5817	20476

Table 8. Core and copper volume used in the separated and integrated transformer-inductor

Total core volume reduction is:

$$\frac{V_{core-integrated}}{V_{core-seperated}} = (1 - \frac{68371.54419}{36989.61643+67706.66146}) \times 100 = 35.33\%$$

Total copper volume reduction is:

$$\frac{V_{copper-integrated}}{V_{copper-seperated}} = (1 - \frac{20476.779093}{5817.570889+20056.356137}) \times 100 = 20.85\%$$

4.1.5 Efficiency

Since the nature of the CLLC and CLLLC converters are different, the size of the resonant capacitance in each converter were different contributing to distinctive switching frequencies in each converter. Besides, the dedicated CLLC coolant system was not ideal one for CLLLC one. Thus, the generated heat by the electromagnetic components was not removed effectively resulting in an increased resistance and causing even more power loss and temperature rise on the winding in CLLLC converter. At boost stage, where the frequency difference in minimum, the archived efficiency is presented in Table 9.

	CLLC	CLLLC
Input voltage (V)	820	820
Output voltage (V)	464	465
Switching frequency (KHz)	80	99.6
Efficiency (%)	96.61	96.12

Table 9. CLLC and CLLLC Efficiency comparison in boost mode

ISBN 978-3-8007-6262-0

However, the best way to compare these two scenarios is to refer to resistance, core loss and volume tables presented in the previous sections.

5 Conclusion

The conclusion of the paper presents a comparative analysis between two 11KW 400V converters, namely the CLLC and CLLLC converters. Throughout the investigation, several key observations were made:
In the CLLC converter, there was a slight shift in resonant frequency compared to the CLLLC converter. Variations in operating points revealed different voltage and current stresses on the components, making it challenging to definitively determine superiority from this aspect alone. The CLLLC converter demonstrated advantages in terms of resistance, core loss, and copper loss over the CLLC converter, primarily due to its smaller size. Notably, the CLLLC converter exhibited a reduced volume of electromagnetic components, leading to significant cost savings and higher power density compared to the CLLC counterpart. Additionally, the CLLLC converter showcased superior EMI behavior compared to the CLLC converter.
In summary, the findings suggest that the CLLLC converter offers several benefits over the CLLC converter, including reduced losses, cost savings, and improved EMI performance, thus making it a promising choice for high-power applications.

References

[1] Dhakar, AK, Soni, A., & Bansal, HO (2020, December). Design and Control of a Bi-directional CLLC Resonant Converter For Low voltage Energy Storage Systems. In 2020 IEEE 17th India Council International Conference (INDICON) (pp. 1-8). IEEE.

[2] Liu, Y., Du, G., Wang, X., & Lei, Y. (2019). Analysis and design of high-efficiency bidirectional GaN-based CLLC resonant converter. Energies, 12(20), 3859.

[3] Joševski, M., Korompili, A., & Monti, A. (2020). Modeling and Voltage Control of Bidirectional Resonant DC/DC Converter for Application in Marine Power Systems. IFAC-PapersOnLine, 53(2), 13056-13063.

[4] Instruments, T. (2018). Survey of resonant converter topologies. In 2018 Texas Instruments Power Supply Design Seminar SEM2300, SLUP (Vol. 376).

[5] Zahid, Z. U. (2015). Design, modeling and control of bidirectional resonant converter for vehicle-to-grid (V2G) applications (Doctoral dissertation, Virginia Tech).

[6] De, D., Klumpner, C., Rashed, M., Patel, C., Kulsangcharoen, P., & Asher, G. (2012, March). Achieving the desired transformer leakage inductance necessary in DC-DC converters for energy storage applications. In 6th IET International Conference on Power Electronics, Machines and Drives (PEMD 2012) (pp. 1-6). IET.

[7] Pavlovsky, M., De Haan, S. W. H., & Ferreira, J. A. (2006, June). Winding losses in high-current, high-frequency transformer foil windings with leakage layer. In 2006 37th IEEE Power Electronics Specialists Conference (pp. 1-7). IEEE.

[8] McLyman, C. W. T. (2004). Transformer and inductor design handbook. CRC press.

[9] Erickson, R. W., & Maksimovic, D. (2007). Fundamentals of power electronics. Springer Science & Business Media.

[10] Ansari, S. A., Davidson, J. N., & Foster, M. P. (2022, June). Fully-integrated transformer with asymmetric leakage inductances for a bidirectional resonant converter. In 11th International Conference on Power Electronics, Machines and Drives (PEMD 2022) (Vol. 2022, pp. 260-265). IET.

[11] Cougo, B., & Kolar, J. W. (2012, March). Integration of leakage inductance in tape wound core transformers for dual active bridge converters. In 2012 7th International Conference on Integrated Power Electronics Systems (CIPS) (pp. 1-6). IEEE.

[12] Steiger, U., & Mariethoz, S. (2010, September). Method to design the leakage inductances of a multiwinding transformer for a multisource energy management system. In 2010 IEEE Vehicle Power and Propulsion Conference (pp. 1-6). IEEE.

[13] Instruments, T. (2020). Bidirectional CLLLC resonant dual active bridge (dab) reference design for HEV/EV on-board charger. Texas Instruments reference design No. TIDM-02002. Accessed Oct, 26.